Available online at www.sciencedirect.com

ScienceDirect

Procedia Structural Integrity 35 (2022) 66–73

Structural Integrity Procedia

www.elsevier.com/locate/procedia

2nd International Workshop on Plasticity, Damage and Fracture of Engineering Materials

A Correlation between Deformation-Induced Surface Roughness and In-Plane Plastic Strain in an Aluminum Alloy at the Mesoscale

V. Romanova[a,*], V. Shakhidzhanov[a], O. Zinovieva[a], O. Nekhorosheva[a,b], R. Balokhonov[a]

[a]*Institute of Strength Physics and Materials Science SB RAS, Tomsk 634055, Russia*
[b]*National Research Tomsk State University, Tomsk 634050, Russia*

Abstract

Experimental and numerical studies on deformation-induced surface roughening in a commercial purity aluminum alloy are presented and discussed. Mesoscale surface profiles evolving in the experimental and numerical specimens in the course of tension are processed to reveal a correlation between roughness characteristics and in-plane plastic strains at the mesoscale. A dimensionless parameter calculated as a ratio of the rough profile length to the profile evaluation length has been used for quantitative estimations of the mesoscale roughness patterns. The dimensionless roughness parameter is shown to depend exponentially on the in-plane plastic strains at the mesoscale. The results support an early assumption that in-plane plastic strains accumulated in a loaded material can be evaluated from the estimations of mesoscale surface roughness.

© 2021 The Authors. Published by Elsevier B.V.
This is an open access article under the CC BY-NC-ND license (https://creativecommons.org/licenses/by-nc-nd/4.0)
Peer-review under responsibility of IWPDF 2021 Chair, Tuncay Yalçinkaya

Keywords: deformation-induced surface roughness; mesoscale; plastic strain, aluminum alloys, crystal plasticity

1. Introduction

Plastic deformation is commonly accompanied by free surface roughening at different scales. Since the early work of Osakada and Oyane (1971), extensive experimental and numerical data on this phenomenon commonly referred to as deformation-induced (DI) surface roughening have been accumulated for polycrystalline metals and alloys. A recent review on this subject is provided, e.g., by Li and Fu (2019). Examination of roughened surfaces

* Corresponding author. Tel.: +7-960-969-2982
E-mail address: varvara@ispms.tsc.ru

2452-3216 © 2021 The Authors. Published by Elsevier B.V.
This is an open access article under the CC BY-NC-ND license (https://creativecommons.org/licenses/by-nc-nd/4.0)
Peer-review under responsibility of IWPDF 2021 Chair, Tuncay Yalçinkaya
10.1016/j.prostr.2021.12.049

with different spatial resolutions has revealed three distinct length scales of out-of-plane surface displacements attributed to different plastic deformation mechanisms. A detailed classification of the multiscale roughening events was given by Raabe et al. (2003). The intragrain displacements related to the slip bands are first to occur as plastic deformation begins. The heights of individual slip steps are comparable to interatomic distance so that even a pack of slip bands are capable of fitting rather limited out-of-plane strain. Thus, further deformation involves larger-scale surface displacements seen as grain clusters conjointly moving up and down relative to each other. The surface patterns formed by the collective grain displacements are classified as mesoscale. Finally, surface waviness is detected at the macroscale with a wavelength comparable to the specimen size. The DI waviness should not be confused with the initial waviness inherited from the sample manufacturing or elastic waviness disappearing after unloading. A pronounced bow-shaped surface region is formed in necking shortly before fracture.

Being well-detected throughout the entire deformation process from the very beginning of plastic deformation to a macroscale necking, the mesoscale roughening events can be utilized in the material stress-strain attestation provided that a correlation between certain characteristics of roughness patterns and plastic strains is established. Since Osakada and Oyane's (1971) pioneering work, many experimental and computational efforts have been made to link the surface morphology with the deformation parameters for different metals and alloys and various loading conditions (e.g., Ma et al. 2019; Messner et al., 2003, 2005; Paul et al., 2019; Shavshukov, 2020; Stoudt et al., 2011; Wang et al., 2013; Yoshida, 2014).

Recently, Romanova et al. (2019a, 2020) have shown on the example of commercial purity titanium that the mesoscale DI roughness was nonlinearly related to in-plane strain through a so-called dimensionless roughness parameter. Being drawn for the particular case, this conclusion still needs further experimental and numerical evidence. This paper continues the experimental and numerical investigations along these lines to reveal a correlation between mesoscale DI roughening and in-plane plastic strains in a commercial purity (CP) aluminum alloy under uniaxial tension.

2. Experimental

2.1. Material

The EBSD map and pole figures for a CP aluminum alloy presented in Fig. 1a and b provide information about the grain shape and orientations. Hereinafter, the X- and Y-axes lie along and transversely to the specimen axis, respectively, and Z-axis is perpendicular to the specimen top plane (Fig. 1c). The microstructure mainly consists of equiaxed grains with the size varied from 20 to 70 μm. The inverse and direct pole figures (Fig. 1a, b) indicate the presence of a two-component texture typical for rolled aluminum {100}<001>+{110}<001> with the cube grains (red colored in Fig. 1a) occupying a larger area.

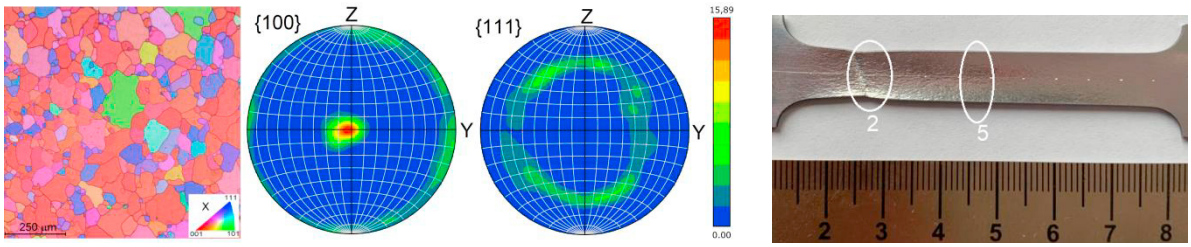

a b c

Fig. 1. EBSD map (a) and pole figures (b) of an aluminum alloy and the experimental specimen after tension (c)

2.2. Stop-and-study measurements

A dog-bone-shaped specimen with a 50×10×1.5 mm^3 gauge part was subjected to quasistatic uniaxial tension using an INSTRON Universal testing machine. In order to reveal a correlation between in-plane plastic strains and

mesoscale deformation-induced roughening, a stop-and-study technique developed by Romanova et al. (2019a) has been utilized.

The specimen gauge section was divided into subsections by a set of control marks indented on the surface along its centerline (Fig.1c). The evaluation length was chosen, relying on the conclusions drawn by Romanova et al. (2019a) for a titanium alloy. In order to be representative of the mesoscale, the surface profile evaluation length should cover ~ 4-5 characteristic wavelengths of the mesoscale surface relief. Our recent experimental and numerical estimations for titanium (Romanova et al. 2019a) showed that the mesoscale clusters initially covering 3 to 5 grains consolidated into 15-20 grain units in the developed deformation stage. Relying on this, 5 mm subsection length was chosen to catch the mesoscale phenomena throughout the entire deformation process. Treating longer profiles is unreasonable since it might lead to averaging the mesoscale roughness effects.

After certain deformation, the specimen was taken from the testing machine to examine strains and roughness profiles in its subsections. The in-plane tensile strain of each subsection was calculated as a ratio of the current distance between the control marks to the reference length of the subsection. In what follows, we denote the strains of the specimen and its subsections by ε and ε_{sub}, respectively. The surface profiles in the subsections were measured by an Alpha-Step IQ contact profiler with a step of 1 μm. Then the specimen was set into the testing machine again and its loading was continued up to the next stop. In such a way, the subsection strains and surface profiles were measured throughout the deformation process with a strain step of 2.5-5%. Along with the periodical profilometry and strain measurements, surface patterns in some selected subsections were treated with a laser scanning microscope NewView.

2.3. Mesoscale roughness quantification

Standardized surface roughness quantification is provided in terms of the arithmetic mean roughness, the root-mean-square roughness and other roughness parameters determined from the deviations of the surface peaks and valleys from the mean line. The roughness evaluation procedure is commonly preceded by filtering the raw surface profiles to remove high-frequency noise oscillations and low-frequency waviness. The resulting roughness estimates are expressed in microns.

Romanova et al. (2017) proposed a new approach to quantify DI roughness in a loaded material, taking into account the origin of this event. Summarizing our previous results (Romanova et al. 2013, 2017, 2019a, 2020) and literature data on DI roughening in metals and alloys (Messner et al., 2003, 2005; Panin et al. 2020; Paul et al. 2019; Qin et al., 2013; Raabe et al., 2003; Shanyavskiy and Soldatenkov, 2020; Stoudt et al., 2011), we came to the conclusion that the rough patterns developing on the free surface under deformation are representative of the multiscale deformation mechanisms involved. In order to take into account the contributions from all length scales appearing within the evaluation length, we estimate mesoscale roughness for unfiltered profiles. By analogy with a strain measure, we have introduced a dimensionless roughness parameter Rd calculated as

$$R_d = \frac{L_r}{L_e} - 1 \tag{1}$$

where L_r is the rough profile length and L_e is the profile evaluation length. Expressed in this way, the roughness parameter is simply calculated and clearly interpreted: the larger is the Rd value, the stronger is the surface irregularity. The free surface of a uniaxially loaded homogeneous material is known to remain flat since no forces act normally to the surface to produce its out-of-plane displacements. Microstructure inhomogeneity in real materials produces nonuniform displacement fields not only along the load axis but also in the perpendicular direction. The latter are related to the surface out-of-plane displacements causing surface roughening in the absence of external forces. Thus, the R_d parameter might reflect a degree of material inhomogeneity to a certain extent.

3. Numerical simulation

Taking in mind that DI surface roughening in real materials is inextricably linked to their structural inhomogeneity, we employ an approach of microstructure-based simulations where the grain structure is taken into account explicitly. For incorporating the grain orientation effects, the constitutive behavior of grains is reasonable to describe in terms of crystal plasticity. The crystal plasticity finite-element approach and its dynamic implementation in simulations of aluminum polycrystals have been validated and discussed at length in many papers (see, e.g., Harewood and McHugh, 2007; Romanova et al., 2019, 2019b). Omitting a detailed mathematical description, let us briefly discuss the main points related to the simulations at hand.

3.1. Polycrystalline model

Based on the experimental data, a polycrystalline model consisting of 1000 equiaxed grains with an average size of 70 μm was generated on a 150×150×50 mesh by the method of step-by-step packing (SSP) (Romanova et al. 2013) and subsequently translated four times along the X-axis and two times along the Y-axis to obtain 3000×1500×250 μm^3 model representative of the mesoscale. As input parameters of the SSP procedure, the grain seeds were randomly distributed over the meshed domain using a random number generator. In the subsequent SSP procedure, the grains were grown in accordance with the equation of a sphere. The resulting grain structure consisting of 8000 grains is shown in Fig. 2a.

Each grain was assigned a Cartesian frame with the axes along the [100], [010] and [001] crystal directions (hereinafter referred to as the crystal frame). The orientations of the local frames with respect to the specimen XYZ-frame (Fig. 2a) were given by a set of Euler angles describing subsequent XYX rotations. The first and the third angles were randomly determined in the range of 180 degrees while the second angle was ranged within 15 degrees in order to fit the experimental texture (cf. Figs. 1b and 2b).

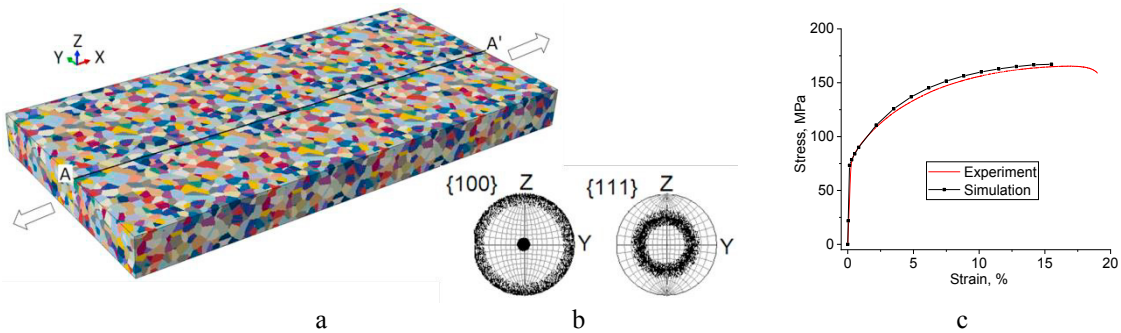

Fig. 2. Grain structure (a) and texture (b) of the model polycrystal and the experimental and numerical stress-strain curves (c).

3.2. Constitutive description, numerical implementation and loading conditions

The dynamic boundary-value problem was solved using Abaqus/Explicit. In the numerical realization, the constitutive equations of grains were formulated with respect to their crystal frames on a consistent basis to relate the stress rate, $\dot{\boldsymbol{\sigma}}$, and the total and plastic strain rates, $\dot{\boldsymbol{\varepsilon}}^T$ and $\dot{\boldsymbol{\varepsilon}}^p$, through the Hooke's law (in order to differ scalar and tensorial quantities, the latter are written in bold type)

$$\dot{\boldsymbol{\sigma}} = \mathbf{C}\left(\dot{\boldsymbol{\varepsilon}}^T - \dot{\boldsymbol{\varepsilon}}^p\right). \tag{2}$$

Here $\dot{\boldsymbol{\varepsilon}}^T$ is calculated through the velocity field provided by the solution to the equation of motion. The plastic strain rate tensor is calculated through a summary slip over active slip systems

$$\dot{\boldsymbol{\varepsilon}}^p = \sum_{\alpha=1..12} \dot{\gamma}^{(\alpha)} \boldsymbol{\theta}^{(\alpha)} \tag{3}$$

where $\boldsymbol{\theta}$ is the tensor defining the α *-th* slip system orientation in the crystal frame and $\dot{\gamma}^{(\alpha)}$ is the slip rate calculated as

$$\dot{\gamma}^{(\alpha)} = a^{(\alpha)} \dot{\gamma}_0 \left| \frac{\tau^{(\alpha)}}{\tau_{CRSS}^{(\alpha)}} \right|^{\nu} sign\left(\tau^{(\alpha)}\right). \tag{4}$$

Here τ is the resolved shear stress, τ_{CRSS} is the critical resolved shear stress (CRSS) necessary to initiate slip, $\dot{\gamma}_0$ is the reference slip rate, ν is the strain rate sensitivity coefficient, a is equal to zero under the CRSS below τ_{CRSS} and turns to 1 otherwise; hereinafter, the superscript in parenthesis denotes the slip system α.

The CRSS value is described by the phenomenological strain hardening function

$$\tau_{CRSS}^{(\alpha)} = \tau_0 + a_1 \left(1 - \exp\left(-\varepsilon_{eq}^p / a_2\right)\right), \tag{5}$$

where τ_0 is the reference CRSS value, ε_{eq}^p is the equivalent plastic strain accumulated in the finite element, and a_1 and a_2 are the approximating constants chosen to fit the experimental stress-strain curve. The material constants and model parameters used in the calculations were C_{1111}=108 GPa, C_{1122}=61 GPa, C_{2323}=28 GPa, τ_0=33 MPa, a_1 =37 MPa, a_2=0.0526. A close agreement between the experimental and numerical stress-strain curves (Fig. 2c) proves the model validation.

In every time step of the numerical implementation, the constitutive equations (2)-(5) were calculated within a VUMAT User Subroutine with respect to the crystal frames and then the stress tensor components were passed to the Abaqus main program to calculate the equation of motion. On the opposite faces perpendicular to the X-axis the displacement velocities were set to simulate uniaxial tension along the X-direction (Fig. 2a). The displacements of the bottom face were constrained in the vertical direction, and the free-surface boundary conditions were set on the top and lateral faces. The tension velocity was smoothly increased and then kept constant to minimize the acceleration effects unnatural for quasistatic processes (see, e.g., Romanova et al. (2019, 2019b) for further details).

4. Results

4.1. Mesoscale roughness patterns

Representative roughness patterns formed in the experimental and model specimens are shown in Figs. 3a and 4a, respectively. Corresponding surface profiles measured in two subsections of the experimental specimen (Fig. 1c) and along the line A-A' in the model polycrystal (Fig. 2a) are plotted in Figs. 3(b, c) and 4b.

The mesoscale roughness patterns became well-defined in the experimental and numerical specimens already in the initial deformation stage. In line with the conclusions made by Romanova et al. (2013, 2017, 2019a) for aluminum and titanium alloys, two distinct rough patterns began to develop simultaneously. Smaller round-shaped hills and dimples associated with the extrusion and intrusion of individual grains and grain clusters relative to the surrounding material are seen in the structure of larger surface undulations formed by extended parallel-like ridges lying by an angle to the axis of tension. Experimental and numerical surface profiles plotted in Figs. 3b-c and 4b additionally confirm that the two kinds of roughness irregularities simultaneously appear on the surface. In the course of deformation, the larger-scale undulations intensify while smaller hills and dimples retard their growth. It is worth noting that the peaks and valleys formed in the early deformation stage evolve under tension but do not change their positions relative to each other.

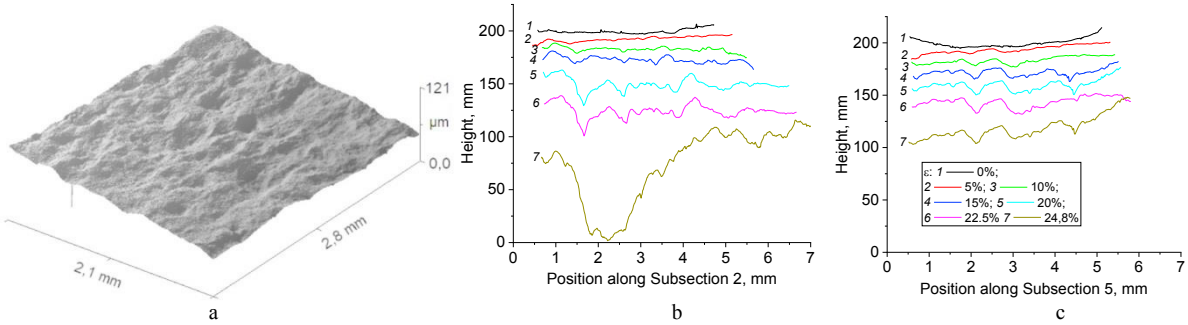

Fig. 3. Experimental surface image (ε_{sub} =18%) (a) and evolution of surface profiles in Subsections 2 (b) and 5 (c) (refer to Fig. 1b).

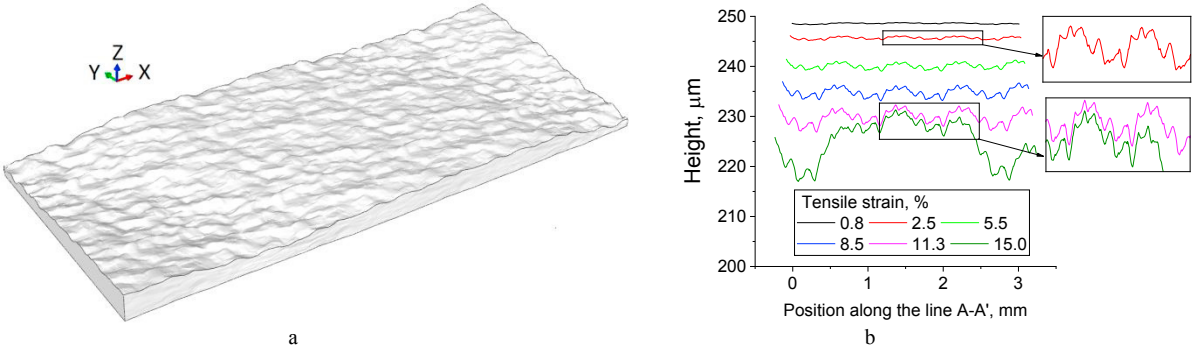

Fig. 4. Calculated roughness pattern at a strain of 15% (a) and surface profiles in the model polycrystal at different strains (b). The Z-displacements in (a) are plotted with a scale factor of 3.

Comparison of the evolving profiles with the grain structure (e.g., cf. Figs. 4b and 2a) suggests that the contributions of surface undulations to the overall roughness patterns are proportional to their characteristic size. The smallest mesoscale irregularities are formed by 3-5 grains and have a period of 200-300 µm. Their heights do not exceed 2-3 µm even in the neck region (Subsection 2 in Fig. 3b). Surface undulations with a characteristic wavelength of 700-1200 µm make a major contribution to roughening throughout the deformation process; their height being of 4-5 µm at 5% strain reaches 30-40 µm in Subsection 2 shortly before necking (Fig. 3b).

4.2. Correlation between mesoscale surface roughness and in-plane plastic strains

For quantitative analysis of the mesoscale roughness patterns, the R_d parameter was calculated by Eq. (1) for the whole set of experimental profiles measured in the ten specimen subsections (Fig. 1b). Totally, 80 experimental profiles were processed to reveal a correlation between the mesoscale roughness and in-plane strains of the corresponding subsections.

The bar graphs in Fig. 5a and b show the dependences of the in-plane strains and R_d values in the subsections on the overall specimen strain. Fig. 5a shows that Subsection 2 where a neck is formed in a later deformation stage begins to deform at a higher strain rate than the other regions as early as 10% overall strain and this tendency is kept throughout the whole deformation process. The strain rate in Subsection 2 demonstrates almost linear growth up to necking (Fig. 5a), while the strains experienced by other subsections slow down or nearly stop growing.

Accordingly, the mesoscale roughness evaluated over all the subsections takes on higher values in Subsection 2 than in the other regions (Fig. 5b). However, the R_d value in Subsection 2 exponentially grows with the specimen strain. The roughness values in other subsections increase modestly in the initial deformation stage and nearly stop growing after 20% specimen strain (see Fig. 5b). Note, the standard roughness estimates generally provide a linear

roughness dependence on the tensile strain (see, e.g., Banovic and Foecke, 2003; Ma et al., 2019; Messner et al., 2003, 2005; Osakada and Oyane, 1971; Stoudt et al. 2011; Wang et al., 2013).

In order to reveal a correlation between the roughness parameter and in-plane plastic strains at the mesoscale, the whole set of the experimental data representing the R_d values versus subsection strains are brought together in Fig. 5c, d. Of importance is the fact that the data obtained for different subsections are perfectly approximated by a single fitting curve with the coefficient of determination equal to 0.99 (the red line in Fig. 5c). The fitting equation is expressed by a sum of two exponential functions

$$\mathrm{R_d} = \left(61.4\exp\left((\varepsilon_{Sub} - 0.1)/0.18\right) + 0.000237\exp\left((\varepsilon_{Sub} - 0.1)/0.027\right) - 34\right)\cdot 10^{-5} \quad (6)$$

The first term of the sum describes the $R_d(\varepsilon_{Sub})$ dependence in the range of moderate plastic strains developing in most specimen regions. The second term is responsible for the catastrophic R_d growth in the neck region due to a contribution from the low-frequency macroscopic waviness component. In the case at hand, this term is negligible for the strains below 20%.

By analogy with the experiment, the R_d values were calculated for numerical profiles measured in the model polycrystal. The numerical strain-dependent roughness curve is plotted in the inset in Fig. 5d in comparison with the experimental data. The R_d dependence, in agreement with the experimental evidence, demonstrates a non-linear growth in the course of deformation. The fact that the numerical and experimental R_d dependences reasonably fit together additionally proves the model validity.

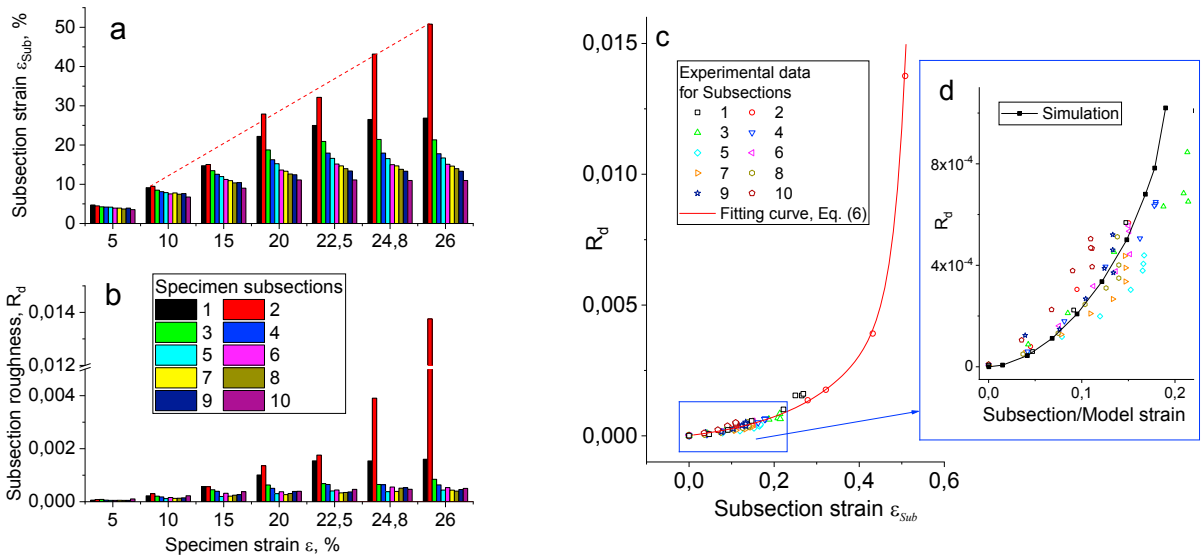

Fig. 5. Subsection strains (a) and roughness values (b) vs. specimen tensile strain, and the R_d values vs. experimental subsection strains (c, d) compared with the numerical data (d).

5. Conclusions

Experimental and numerical studies were performed to reveal a correlation between mesoscale deformation-induced surface roughness and in-plane plastic strains in a polycrystalline aluminum alloy under uniaxial tension. The roughness evolution was investigated throughout the specimen surface in a wide range of tensile strains. A dimensionless roughness parameter R_d calculated as a ratio of the rough profile length to the profile evaluation length was used to quantify roughness patterns developing at the mesoscale.

The R_d values calculated for a set of mesoscale surface profiles were shown to depend exponentially on the in-plane strains of the evaluated regions. A strong correlation between the mesoscale dimensionless roughness

parameter and in-plane plastic strains has been revealed to confirm that plastic strain accumulated in a material can be evaluated from estimations of mesoscale deformation-induced roughness. Particularly, in the experiments presented in this study, the place of necking was predicted pretty in advance of its visible manifestation at the macroscale from the comparison of R_d values in the specimen subsections.

Acknowledgements

This work is supported by Russian Science Foundation through the grant № 20-19-00600. The microstructures were generated using the in-house software "SSP-design" developed according to the Government research assignment for ISPMS SB RAS, project FWRW-2021-0002. EBSD-data were obtained at Equipment Center for Collective Use at Tomsk State University.

References

Banovic, S.W., Foecke, T., 2003. Evolution of Strain-Induced Microstructure and Texture in Commercial Aluminum Sheet under Balanced Biaxial Stretching. Metall. Mater. Trans. A. 34, 657–671.

Harewood, F.J., McHugh, P.E., 2007. Comparison of the Implicit and Explicit Finite Element Methods using Crystal Plasticity. Comput. Mater. Sci. 39, 481–494.

Li, H., Fu, M., 2019. Inhomogeneous Deformation-Induced Surface Roughening Defects, in "*Deformation-Based Processing of Materials*". Elsevier, pp. 225–256.

Ma, X., Zhao, J., Du, W., Zhang, X., Jiang, Zh., 2019. Analysis of Surface Roughness Evolution of Ferritic Stainless Steel using Crystal Plasticity Finite Element Method. J. Mater. Res. Technol. 8(3), 3175–3187.

Messner, C., Oberndorfer, C., Werner, E.A., 2005. Surface Roughness of Duplex Steels: Role of the Microstructure. Comput. Mater. Sci. 32(3-4), 455–462.

Messner, C., Silberschmidt, V.V., Werner, E.A., 2003. Thermally Induced Surface Roughness in Austenitic–Ferritic Duplex Stainless Steels. Acta Mater. 51, 1525–1537; https://doi.org/10.1016/s1359-6454(02)00545-1

Osakada, K., Oyane, M., 1971. On the Roughening of Free Surface in Deformation Processes. Bull. JSME 14, 171–177.

Panin, V.E., Egorushkin, V.E., Kuznetsov, P.V., Galchenko, N.K., Shugurov, A.R., Vlasov, I.V., Deryugin, Ye.Ye., 2020. Structural Turbulence of Plastic Flow and Ductile Fracture in Low-Alloy Steel under Lattice Curvature Conditions. Phys. Mesomech. 23, 279–290.

Paul, S.K., Roy, S., Sivaprasad, S., Tarafder, S., 2019. Forming Limit Diagram Generation from In-Plane Uniaxial and Notch Tensile Test with Local Strain Measurement through Digital Image Correlation. Phys. Mesomech. 22, 340–344.

Qin, L., Seefeldt, M., Van Houtte, P., 2013. Meso-Scale Modelling on Ridging or Roping of Aluminium Alloys. Mater. Sci. Technol. (MS&T) 2013 2, 1274–1283.

Raabe, D., Sachtleber, M., Weiland, H., Scheele, G., Zhao, Z., 2003. Grain-Scale Micromechanics of Polycrystal Surfaces during Plastic Straining. Acta Mater. 51, 1539–1560.

Romanova, V.A., Balokhonov, R.R., Batukhtina, E.E., Emelianova, E.S., Sergeev, M.V., 2019. On the Solution of Quasi-Static Micro- and Mesomechanical Problems in a Dynamic Formulation. Phys Mesomech 22, 296–306.

Romanova, V., Balokhonov, R., Emelianova, E., Pisarev, M., Dymnich, E., 2020. Numerical Study of the Texture Effect on Deformation-Induced Surface Roughening in Titanium Polycrystals. Eng. Fail. Anal. 110, 104437.

Romanova, V., Balokhonov, R., Emelianova, E., Sinyakova, E., Kazachenok, M., 2019a. Early Prediction of Macroscale Plastic Strain Localization in Titanium from Observation of Mesoscale Surface Roughening. Int. J. Mech. Sci. 161–162, 105047.

Romanova, V., Balokhonov, R., Emelianova, E., Zinovieva, O., Zinoviev, A., 2019b. Microstructure-Based Simulations of Quasistatic Deformation Using an Explicit Dynamic Approach. Facta Universitatis. Ser. Mech. Eng. 17(2), 243–254.

Romanova, V., Balokhonov, R., Panin, A., Kazachenok, M., Kozelskaya, A., 2017. Micro- and Mesomechanical Aspects of Deformation-Induced Surface Roughening in Polycrystalline Titanium. Mater. Sci. Eng. A 697, 248–258.

Romanova, V.A., Balokhonov, R.R., Schmauder, S., 2013. Numerical Study of Mesoscale Surface Roughening in Aluminum Polycrystals under Tension, Mater. Sci. Eng. A. 564, 255–263.

Shanyavskiy, A.A., Soldatenkov, A.P., 2020. Scales of Metal Fatigue Limit. Phys. Mesomech. 23, 120–127.

Shavshukov, V.E., 2020. Extreme Strain Fluctuations in Polycrystalline Materials. Phys. Mesomech. 23, 13–20.

Stoudt, M.R., Levine, L.E., Creuziger, A., Hubbard, J.B., 2011. The Fundamental Relationships Between Grain Orientation, Deformation-Induced Surface Roughness and Strain Localization in an Aluminum Alloy. Mater. Sci. Eng. A 530, 107–116.

Trusov, P.V., Sharifullina, E.R., Shveykin, A.I., 2019. Multilevel Model for the Description of Plastic and Superplastic Deformation of Polycrystalline Materials. Phys. Mesomech. 22, 402–419.

Wang, Y, Meletis, E.I., Huang, H., 2013. Quantitative Study of Surface Roughness Evolution during Low-Cycle Fatigue of 316L Stainless Steel using Scanning Whitelight Interferometric (SWLI) Microscopy. Int. J. Fatigue 48, 280–288.

Yoshida, K., 2014. Effects of Grain-Scale Heterogeneity on Surface Roughness and Sheet Metal Necking. Int. J. Mech. Sci. 83, 48–56.